Senescence-associated ß-galactosidase staining over the lifespan differs in a short- and a long-lived fish species

Simon Schöfer,[1]* Sylvia Laffer,[1]* Stefanie Kirchberger,[2] Michael Kothmayer,[1] Renate Löhnert,[1] Elmar E. Ebner,[1] Klara Weipoltshammer,[1] Martin Distel,[2] Oliver Pusch,[1] Christian Schöfer[1]

[1]Department for Cell and Developmental Biology, Center for Anatomy and Cell Biology, Medical University of Vienna
[2]St. Anna Children's Cancer Research Institute (CCRI), Vienna, Austria

*These authors contributed equally

ABSTRACT

During the aging process, cells can enter cellular senescence, a state in which cells leave the cell cycle but remain viable. This mechanism is thought to protect tissues from propagation of damaged cells and the number of senescent cells has been shown to increase with age. The speed of aging determines the lifespan of a species and it varies significantly in different species. To assess the progress of cellular senescence during lifetime, we performed a comparative longitudinal study using histochemical detection of the senescence-associated beta-galactosidase as senescence marker to map the staining patterns in organs of the long-lived zebrafish and the short-lived turquoise killifish using light and electron microscopy. We compared age stages corresponding to human stages of newborn, childhood, adolescence, adult and old age. We found tissue-specific but conserved signal patterns with respect to organ distribution. However, we found dramatic differences in the onset of tissue staining. The stained zebrafish organs show little to no signal at newborn age followed by a gradual increase in signal intensity, whereas the organs of the short-lived killifish show an early onset of staining already at newborn stage, which remains conspicuous at all age stages. The most prominent signal was found in liver, intestine, kidney and heart, with the latter showing the most prominent interspecies divergence in onset of staining and in staining intensity. In addition, we found staining predominantly in epithelial cells, some of which are post-mitotic, such as the intestinal epithelial lining. We hypothesize that the association of the strong and early-onset signal pattern in the short-lived killifish is consistent with a protective mechanism in a fast growing species. Furthermore, we believe that staining in post-mitotic cells may play a role in maintaining tissue integrity, suggesting different roles for cellular senescence during life.

Key words: SA-ßGal; teleost; senescence; aging; *Nothobranchius furzeri*; *Danio rerio*.

Correspondence: Christian Schöfer, Department for Cell and Developmental Biology, Center for Anatomy and Cell Biology, Medical University of Vienna, Schwarzspanierstr. 17, 1090 Vienna, Austria. Tel. +43.1.40160-37713. E-mail: christian.schoefer@meduniwien.ac.at

Contributions: the study was conceptualized by CS, KW, OP; experiments were mainly performed by SS, SL with contributions from CS. Animal provision and intellectual input from EEE, MK, RL, SK, MD. Data analysis was mainly done by SS, KW, CS with input from SL. Manuscript drafting by CS with intellectual input by all authors. All the authors read and approved the final version of the manuscript and agreed to be accountable for all aspects of the work.

Conflict of interest: the authors declare no conflict of interest, and all authors confirm accuracy.

Ethics approval: the animal experiment was approved by the Austrian Federal Ministry of Education, Science and Research (GZ: BMWFW-66.009/0031-V/3b/2019). Killifish rearing is licensed under BMBWF-66.009/0130-V/3b/2018 (Austrian Federal Ministry of Education, Science and Research) and zebrafish rearing under GZ:565304/2014/6 of the local authorities (Vienna municipal administration MA58).

Availability of data and materials: the datasets are available from the corresponding author upon reasonable request.

Funding: the study was supported by the Austrian Science Fund (FWF)/Herzfelder'sche Familienstiftung grants P30642-b28 (to CS) and P34191 (to OP).

Introduction

Aging is the consequence of a complex interplay of external stimuli and cell-autonomous factors with cellular damage as a key factor.[1] Damaged nuclear or cytoplasmic molecules accumulate in cells, causing the cells to permanently exit the cell cycle[2] but remain viable, a state known as cellular senescence. Senescent cells exhibit morphological and molecular signatures that distinguish them from other non-dividing cells, such as quiescent cells.[3] Cellular senescence can be triggered by a variety of stress factors, such as telomere attrition, mitochondrial dysfunction, cell damage by free radicals, UVB light, µ-irradiation, or chemotherapeutic drugs, hence a tumor-suppressive function of senescence has been proposed.[4-11] Accordingly, an increase in senescent cells with age has been demonstrated both in cultured cells and in many organisms, including humans.[11-16] In addition, the targeted removal of senescent cells (senolysis) in mice led to better health and an increased lifespan.[17-21] However, the relation between age and number of senescent cells is complex, as senescent cells have also been shown to be beneficial under physiological conditions such as in wound healing, tissue repair, developmental processes[22-26] and are required for the functionality of normal adult tissues such as the liver.[27] The ambivalent roles of senescent cells are emphasized by a study in humans that showed that senescence-associated genes associate with anti-longevity, while anti-senescence-associated genes correlate rather with longevity.[16] Cellular senescence is characterized by significant changes in gene expression, such as downregulation of DNA repair factors, upregulation of senescence-induced heterochromatin factors and the compensatory upregulation of pro-mitotic signals, whereby senescent cells remain in an arrested but hyperactive state.[28] A prominent feature of senescent cells is an altered secretome, termed the "senescence-associated secretory phenotype" (SASP), which is associated with an increase in number, size and activity of lysosomes.[18,29] Paracrine secretion from senescent cells has been demonstrated to influence neighboring cells to also enter a senescent state (bystander senescence).[30,31] Progress in better understanding cellular senescence is hampered by the lack of unique markers of aging and senescence.[32,33] In the absence thereof, surrogate markers are used to identify cellular processes that are known to be altered in aging cells. For microscope-based studies, the histochemical reaction for the detection of senescence-associated beta galactosidase (SA-ßGal, SABG) is widely used, which results in a dark blue precipitate.[34-36] SA-ßGal is an important enzyme of lysosomes and a component of SASP and is therefore highly expressed in senescent cells. The exact relationship between SA-ßGal expression levels and aging is not well understood, but it has been shown that SA-ßGal staining is closely related to the development of cellular senescence, *i.e.* it increases with age.[13,34-38] The rate of aging determines the lifespan of an organism and varies greatly from organism to organism. Therefore, it is tempting to compare the SA-ßGal reaction in tissues of a long-lived and a short-lived species during their lifetime. In this study, we used two teleost fish aging model systems, the long-lived zebrafish *Danio rerio*[39,40] and the short-lived turquoise killifish *Nothobranchius furzeri* (further named "killifish";[41]) with maximum survival rates of 60 months and 19 weeks, respectively. In zebrafish, SA-ßGal whole-mount and tissue staining at different ages showed a gradual overall increase of senescence with age in the skin,[42-44] intestine and testis[45] and in brain.[46] In telomerase null-mutant zebrafish, SA-ßGal-positive cells accumulated in intestine, testis, kidney and skeletal muscle.[45,47] In killifish, age-dependent increase in SA-ßGal staining in the brain[48,49] and in the skin[41,50,51] has been reported. Age-dependent increase in SA-ßGal-positive cells was also found in the closely related annual fish *N. guentheri* in the skin, intestine and ovary.[52-54] A comprehensive microscopy-based study of SA-ßGal-staining in zebrafish and killifish is lacking. Here, we present a comparative interspecies study at light and electron microscope level across organs and tissues over the entire lifespan for both species, the short-lived killifish and the long-lived zebrafish at corresponding age stages.

Materials and Methods

Fish husbandry

D. rerio and *N. furzeri* (strain GRZ) were maintained in two independent facilities, both certified by national agencies. Zebrafish were reared in a research fish facility (Tecniplast, Buguggiate, VA, Italy) at the CCRI under license GZ:565304/2014/6 of the local authorities (Vienna municipal administration MA58) and killifish in a facility at the Center for Anatomy and Cell Biology under license BMBWF-66.009/0130-V/3b/2018 (Austrian Federal Ministry of Education, Science and Research). The zebrafish were kept under standard conditions,[55] while killifish were fed a diet of nauplia larvae (newborns) and *Chironomus* larvae (older stages). The killifish were kept under 12-h dark-light cycle at a constant temperature of 28°C. Under these husbandry conditions, the majority of killifish (90%) have a maximum survival time of 19 weeks from hatching to death.[56]

Selection of age stages

We analyzed age stages that roughly correlate with each other, taking into account the very different lifespans of Nf and Dr, and analyzed organs corresponding to human age stages (zebrafish stages according to Kimmel *et al*.[55] and Gilbert *et al*.[57]). The age of zebrafish was counted from fertilization (days post-fertilization, dpf). Under the standard conditions used they hatch 2-3 days later. Killifish have a much longer embryonic developmental time as a consequence of evolutionary adaptation to environmental conditions (life in temporary pools), and counting began at hatching (days post-hatching, dph). Thus, human newborn age corresponds to 4 dph for killifish and 5 days dpf for zebrafish, childhood to 3 weeks for killifish and 6 weeks for zebrafish, adolescence to 5 weeks for killifish and 6 months for zebrafish, adulthood to 12-13 weeks for killifish and 15 months for zebrafish, old age to 18-20 weeks for killifish and 26 months for zebrafish.

Tissue handling

Depending on the size of the animals, the fish were either processed *in toto*, *i.e.* in the case of killifish at the ages of 4 dph (newborns), 3 weeks (children) and 5 weeks (adolescents), and in the case of zebrafish at ages of 5 days dpf (newborns) and 6 weeks dpf (children). Animals were killed using 400 mg/L MS-222 (tricain). In older animals, the gut tube, liver, heart, brain, kidneys, skeletal muscle and gonads were isolated and further processed. At least three animals were processed for each species/age (n=3). All fish/organs were fixed overnight with 4% paraformaldehyde, washed with PBS, embedded in cryomolds with O.C.T. compound (Tissue-Tek; Sakura Finetek, Nagano, Japan) and placed on dry ice. Cryosections were processed for histochemistry; for immunofluorescence, the intestines of killifish, fixed as above, were embedded in paraffin.

Immunofluorescence staining

Proliferating cells in the intestine were detected on paraffin sections using a mouse anti-PCNA antibody (RRID:AB_628110; Santa Cruz Biotechnology, Dallas, TX, USA), diluted 1:50-1:100 at 4°C overnight, followed by a goat anti-mouse Alexa488 secondary antibody (Invitrogen, Waltham, MA, USA), diluted 1:500 -1:1000

at room temperature for 30 min with prior antigen retrieval (HIER; 30 min steaming with 10 mM citrate buffer, pH = 6.0). Thereafter, we performed autofluorescence quenching using TrueView (Vector Laboratories, Newark, CA, USA) prior to counterstaining with DAPI (0.1 µg/mL at room temperature for 6 min); a coverslip was mounted with Vectashield (Vector Laboratories). The primary antibody was omitted for negative controls (*not shown*).

Dextran labeling of kidneys

A protocol established for zebrafish was applied to adult male killifish.[58] To minimize harmful interventions only one (male) individual was used (n=1). The fish was anesthetized with 100 mg/L tricaine (MS-222) and received an intraperitoneal injection of 15 µL of a 50 mg/mL solution of a dextran-RITC (Wt 9400, Sigma R8881; Sigma-Aldrich, St. Louis, MO, USA) in deionized water before returning to the tank. 24 h later, kidneys were harvested, fixed overnight in 4% paraformaldehyde and processed for cryosectioning as described above. The sections were used for SA-ßGal staining as below.

SA-beta Gal staining on cryosections

The SA-ßGal enzyme hydrolises beta galactosides into monosaccharides. The most commonly used experimental substrate for SA-ßGal reactivity is XGal (5-bromo-4-chloro-3-indolyl-ß-D-galactopyranoside), which is catalysed by SA-ßGal into galactose and 5-bromo-4-chloro-3-hydroxyindole, producing an indigo-blue precipitate. As a lysosomal enzyme, it is ubiquitously present in cells and can be detected in most cells at pH=4.0. The reaction is carried out at pH=6.0 in order to achieve better selectivity for the highly SASP-active senescent cells.[59] A commercially available staining kit (Cell Signaling Technology, Danvers, MA, USA; #9860) was used according to the manufacturer´s instructions. Briefly, slides were washed in distilled water, then in PBS, and incubated overnight in a sealed chamber with ß-galactosidase staining solution. Care was taken to adjust the pH value of the latter to 6.0. Shorter incubation times reduced the signal intensities but did not alter the staining patterns. After short washes of slides with PBS, slides were immersed in PBS containing DAPI and the coverslips were mounted with Citifluor (EMS, Hatfield, PA, USA). These last steps were performed in horizontal orientation to reduce detachment of cryosections from glass slides. DAPI (0.1 µg/mL; room temperature, 6 min) was used to identify unstained tissues under the microscope. In this way, interference in intensity measurements was avoided between SA-ßGal precipitates and a counterstain in transmitted light-mode.

SA-beta Gal staining for electron microscopy

For ultrastructural analysis of SA-ßGal staining, we applied an *en-bloc* protocol for the detection of XGal in transgenic mice at electron microscopy level with minor modifications.[60] Briefly, we prepared small pieces of tissue of sizes suitable for TEM and fixed these pieces with 2.5% glutaraldehyde + 1% paraformaldehyde + 1% sucrose in PBS for 3 h at room temperature. After washing in PBS, the tissue blocs were transferred to PBS adjusted to pH=6.0 and then subjected to the SA-ßGal reaction overnight as described above. After washing with PBS and deionized water, the blocs were post-fixed with 1% aqueous osmium tetroxide for 1 h, washed with deionized water, dehydrated in an ascending series of ethanol incubations (10 min each), transferred to propylene oxide for 1x 5 min and 1x 2 min and a 1:1 mixture (v:v) of propylene oxide and Epon812 for 30 min and then incubated overnight in pure Epon812. The blocs were then cured at overnight 60°C. Semithin sections of 350 nm thickness were cut, imaged, counterstained with toluidine blue and imaged again. The dark blue color of toluidine blue could easily be distinguished from the turquoise-light blue color of the SA-ßGal reaction. For EM, ultrathin sections were cut at 70 nm and contrasted with 1% uranyl acetate (methanol) and lead citrate.

Imaging

Images of the stained cryosections were acquired with an Evident VS120 automated slide scanning system. First, a fluorescence overview image (DAPI) of the entire slide was recorded to identify all organs. Subsequently, images of identical areas were taken in transmitted light mode to capture the SA-ßGal staining using a 40x NA1.3 dry lens. All transmitted light images were acquired with identical exposure time and saved as 8-bit images in the proprietary .vsi file format. The images were viewed and appropriate positions for measurements were selected with VS Desktop software (Evident). Selected areas were copied to the clipboard and transferred to image analysis software (see below). Semithin sections were captured using a Nikon (Tokyo, Japan) Eclipse800 microscope with a 100x NA1.4 immersion oil lens and saved in .jpg file format. Images of the ultrastructure were taken on a FEI Tecnai G2 20 TEM and saved in .tif file format.

Image evaluation and data processing

The morphological characterization of zebrafish and killifish sections was based on Menke *et al*.[61] and Dykova *et al*.[62] Differing staining patterns of SA-ßGal per organ were observed: in the liver, a relatively homogenous staining was observed across the entire organ, whereas most other organs showed positive signal in cell accumulations, or in certain structures or in certain tissues within organs that resulted in a heterogeneous staining pattern. In both cases, signal intensities were different at different age stages. To account for those differences, we adapted the principle of Allred scoring,[63] which is known from pathology, where it is typically used to evaluate immunohistochemical reactivity patterns across mammary tissue sections. This semi-quantitative evaluation method considers three parameters: a) the proportion of positive cells of all cells; b) the overall signal intensity of the sectioned organ; and c) the signal intensity of positive cells only. The categories for the staining patterns for parameter a (*i.e*., the ratio of positive cells to all cells) were: 0 none, 1 <1:100, 2 1:100-1:10, 3> 1:10 and for parameters b and c: 0 none, 1 weak, 2 intermediate and 3 strong. Blinded evaluation was performed by two investigators. In addition to this semi-quantitative approach, we performed grey value density measurements of the organ overall intensity per section and the intensity of the positives therein (parameters b, c from above). Suitable image areas were selected in the VS Desktop software and transferred to the open-source software Fiji,[64] where all measurements were done on images with 8-bit color depth. For measurements on whole organs (parameter b), the sectioned area of an organ was manually outlined using the DAPI image as reference and mean grey density was measured; an area outside was measured for background density. For measurement of intensities of positives (parameter c), the color thresholding mode of Fiji was applied by manually adjusting the color sliders to select appropriate "blueness" (hue) values in the blue color space and adjusting the brightness to select only the cells and areas with SA-ßGal staining (Otsu thresholding). The generated mask was used to measure the mean grey values on the original image. The measured mean grey values were transferred to a spreadsheet program (Microsoft Excel®). The grey values were inverted and the background was subtracted from measured values. The resulting values were expressed as percentage of black (255; inverted). We used Adobe® Photoshop to arrange figures and Microsoft PowerPoint® for the final design and labelling.

Results

Evaluation of SA-ßGal staining

The staining pattern was different in the investigated organs: a homogeneous distribution of positive cells was only found in liver, while the other organs displayed a heterogeneous pattern, *i.e.*, only some cells, structures or tissues were positive within an organ. At the same time, we also found differences in the signal intensity of the positive cells, with all these parameters varying over the lifetime. For quantification, we found that the Allred scoring system,[63] which is used for immunohistochemical evaluation in pathology, best covers the observed staining patterns. It takes into account the proportion of positive cells of all cells in a section of an organ as well as the signal intensity of positive cells. In addition, the scoring asks for the signal intensity in the whole section of the organ, which can be considered as a function of the aforementioned parameters (Figure 1). Since, to our knowledge, Allred scoring has not yet been applied to SA-ßGal staining, we wanted to compare the results of the semi-quantitative Allred scoring, which was performed by two individuals in a double-blinded fashion, with a second, independent and quantitative approach. For this purpose, we performed intensity measurements on whole sections and on only positive cells (Figure 2 B,C; Supplementary Figure 1A). Comparison of the results of both approaches with respect to these two parameters yielded concordant results, suggesting that double-blinded Allred scoring is a suitable evaluation strategy that covers most aspects of the observed staining patterns.

General SA-ßGal staining patterns

SA-ßGal staining varied considerably between organs, along lifetime and between the two species (Figure 2A). In some organs, the signal intensity varies substantially throughout lifetime, while others are rather constantly stained during life. In other tissues little or no signal is detectable even at old age. For example, in killifish, the heart shows high intensity staining throughout lifetime, whereas skeletal muscle displays very low staining until old age. Unexpectedly, some tissues in killifish already showed reactivity in newborns, while in others an increase was observed toward adulthood and old age. Interspecies comparison across the lifespan revealed that the intensity of staining in zebrafish was generally much lower and occurred much later in life than in killifish. An extreme example is the heart, which in killifish shows strong signal from the newborn stage onwards but in zebrafish remains almost undetectable until adulthood. However, the signal pattern in the same organs were remarkably similar in both species. Measurement of grey values over the entire organ section and of intensities of positive cells revealed a general pattern of increasing staining with age, from low to absent signal in the newborn stage to adulthood, where a slight but significant decrease can be observed (exception gonads), before the staining intensity increases again towards old age stage (Figure 2 B,C; Supplementary Figure 1A). The proportion of positive cells in all cells remains relatively constant in all organs along the lifespan, which indicates tissue specificity of SA-ßGal staining. An exception is the liver and, to a lesser extent, the brain, where the proportion increases significantly with age.

SA-ßGal staining in the intestine

The stomach-less gut tube of both species forms a relatively simple bended tube with an inner relief of folds and intervening interfold regions.[65] We focused on the small intestine and found prominent SA-ßGal staining in the epithelial lining of the folds where both enterocytes and goblet cells were stained (Figure 3 A,B). Closer inspection revealed that the positive signal in killifish was restricted to the apical segment of cells, where the release of beta-galactosidase through the apical membrane was observed (Figure 3C). It is noteworthy that the interfold regions were devoid of SA-ßGal staining. Immunofluorescence labelling to detect proliferating cells (PCNA) identified these regions as those where cell divisions occur in the intestinal epithelia (Supplementary Figure 2B). Apart from the epithelial lining, single positive cells were scattered through the lamina propria, possibly representing

organ	species	score	newborn	childhood	adolescence	adult	old age
intestine	Nf	proportion	2	2	2	2	2
		Int. overall	1	2	2	2	2
		Int. pos	1	2	2	2	2
	Dr	proportion	0	0	1	1	1
		Int. overall	0	0	1	1	1
		Int. pos	0	0	1	1	1
liver	Nf	proportion	0	2	3	3	3
		Int. overall	0	1	2	2	2
		Int. pos	0	1	2	2	3
	Dr	proportion	0	0	0	1	1
		Int. overall	0	0	0	0	0
		Int. pos	0	0	1	1	1
heart	Nf	proportion	3	3	3	3	3
		Int. overall	2	2	2	2	3
		Int. pos	2	3	3	3	3
	Dr	proportion	0	0	0	0	1
		Int. overall	0	0	0	0	0
		Int. pos	0	0	0	0	1
brain	Nf	proportion	0	1	2	2	2
		Int. overall	0	1	1	1	2
		Int. pos	0	1	1	1	2
	Dr	proportion	0	0	0	0	1
		Int. overall	0	0	0	0	1
		Int. pos	0	0	0	0	1
kidney	Nf	proportion	1	2	2	2	2
		Int. overall	1	1	1	1	2
		Int. pos	1	2	2	2	2
	Dr	proportion	0	0	1	0	1
		Int. overall	0	0	0	0	2
		Int. pos	0	0	1	0	1
skel_mu	Nf	proportion	0	0	0	0	1
		Int. overall	0	0	0	0	0
		Int. pos	0	0	0	0	1
	Dr	proportion	0	0	0	0	0
		Int. overall	0	0	0	0	0
		Int. pos	0	0	0	0	0
gonad	Nf	proportion	gnf	1	1	2	2
		Int. overall	gnf	1	1	1	2
		Int. pos	gnf	1	1	2	2
	Dr	proportion	gnf	gnf	0	1	1
		Int. overall	gnf	gnf	1	0	0
		Int. pos	gnf	gnf	1	1	1

Figure 1. Semi-quantitative Allred score of killifish (Nf) and zebrafish (Dr) organs. Proportion of positive cells in all cells: score 0/grey – no positive cells, score 1/yellow - positive:negative <1:100, score 2/green - positive:negative between <1:100 and 1:10, score 3/red - positive:negative > 1:10; overall intensity/intensity of positives: score 0/grey – intensity=0, score 1/yellow – intensity=weak, score 2/green – intensity=medium, score 3/red – intensity=high; gnf, gonads not found.

immune cells. The intensity of whole organ and positive cell signal increases from newborns towards adolescent animals, followed by a characteristic attenuation in adulthood, before increasing again towards old age (Figures 1 and 2 B,C; Supplementary Figures 1A and 2A). Staining in the colon was similar but we observed a higher signal intensity at early age when compared to the small intestine (*data not shown*). When PCNA staining is compared with SA-ßGal, the SA-ßGal staining begins incipient with terminal differentiation into enterocytes and goblet cells. It will be interesting to investigate whether senescence triggers the exit of transient-amplifying cells from cell cycle or whether senescence is a consequence of cell cycle exit, as the SA-ßGal staining persists while cells migrate upwards on the fold.

SA-ßGal staining in the liver

Both species lack liver lobules known from mammals and no periportal fields are present. SA-ßGal staining was present in single cells homogeneously distributed throughout the liver parenchyma (Figure 3D). Interestingly, we never observed cluster formation of positive cells. Closer examination revealed that positive cells were indeed hepatocytes (Figure 3 E,F). In addition, particles could be seen in the space of Disse and in liver sinusoids, suggestive of secretion from hepatocytes. No signal was observed in other cells, such as fibroblasts, although isolated fibroblast cells from zebrafish liver were shown to stain positively *in vitro* in late passage cell culture.[66] In case of killifish liver, all evaluated parameters showed an increase from newborn to adulthood, reaching a plateau in adulthood and an increase toward old age. In zebrafish, staining was only detectable from adolescence onwards and then showed the same characteristics as in killifish, albeit at a lower intensity level (Figures 1 and 2 B,C; Supplementary Figures 1A,B and 2A).

SA-ßGal staining in the heart

The morphology of the heart of zebrafish has been described as consisting of an unseptated atrium, ventricle and bulbus arteriosus.[67] The ventricular wall shows intense trabeculation (hypertrabeculation compared to endothermal hearts) with a comparatively thin compact myocardial layer.[68] The killifish heart has not been described yet but we found a similar morphology to zebrafish. The heart was consistently the most intensely stained organ, and the signal intensity was always significantly higher in killifish than in zebrafish. The staining was stronger in the ventricle than in the atrium. On closer inspection, we found that the signal was strongest in the endocardial epithelial lining, where all cells were strongly positively stained. Cardiomyocytes were not or weakly stained in the centers of the cells, but showed an increased staining towards the periphery of cells lying directly beneath the endocardial epithelial cells (Figure 3G). Staining could also be found adjacent to the cell membrane of the endocardial cells, indicating galactosidase release. The signal at the basal side of endocardial cells appears to diffuse into the neighbouring cardiomyocytes, leading to a denser signal at the periphery of myocytes. Of note, we did not observe signal in the nuclear envelope space and endoplasmic reticulum of myocytes, suggesting that endothelial cells are the source of staining in myocytes. Within the myocytes, the signal appears to penetrate into the myofibrils of the *en-bloc* processed tissue (Figure 3 H,I). Interestingly, the hearts of newborn killifish already showed strong signal, which persisted until adulthood, followed by a significant increase in staining at old age. In stark contrast, the hearts of zebrafish were negative most of the time and only showed some staining at old age, although that was significantly below signal intensity of killifish (Figures 1 and 2 B,C; Supplementary Figures 1A and 2A). This difference can be seen as a rather extreme temporal shift in the onset of beta-galactosidase expression between the two species. Other cardiac cells known to become senescent in mammals were not stained, such as cardiac blood vessel endothelial cells or fibroblasts, although isolated mammalian cardiac fibroblasts are known to acquire staining *in vitro* at late passages.[66]

SA-ßGal staining in the brain

The structure of the zebrafish brain has been intensively studied and well documented.[69] For the killifish brain, an increase in SA-ßGal staining throughout lifetime has been reported, along with an increase in many parameters of aging-related neurodegenerative diseases.[39,49] In line with these reports, we found staining restricted to distinct cell groups, likely neuronal nuclei (Figure 4 A,B). These clusters were found in the brain stem in killifish, while the prominent optic tectum was not stained. In newborn killifish,

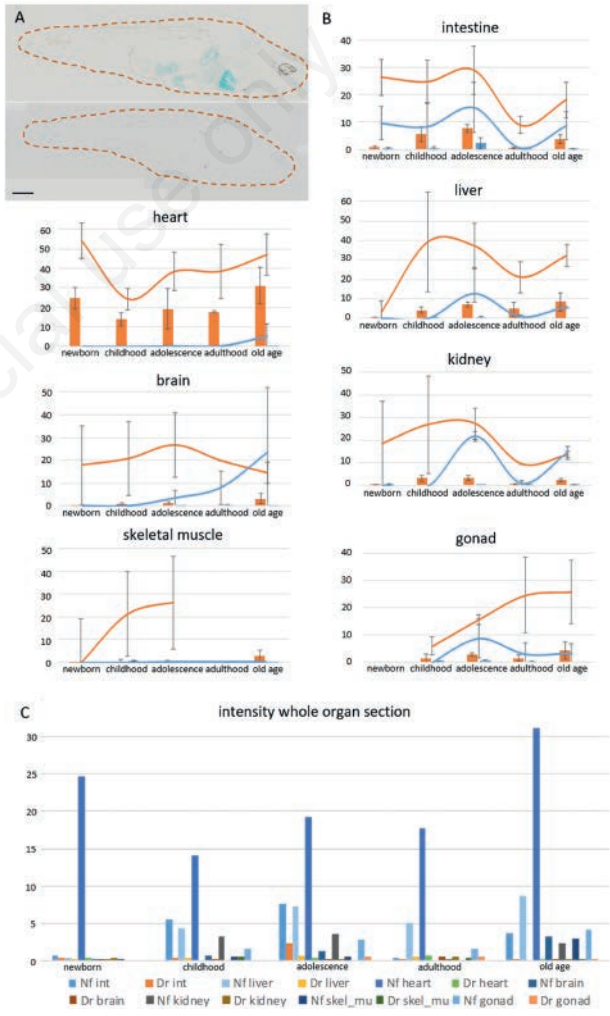

Figure 2. Quantitative intensity measurements in killifish (Nf) and zebrafish (Dr) organs along lifespan. **A**) representative examples of SA-ßGal staining in fish in childhood age; upper panel: Nf (3 weeks), lower panel: Dr (6 weeks); contour of sectioned fishes indicated as dashed line. **B**) Quantifications of overall intensity over the organ section (bars) and of intensity of positive cells only (lines); Nf in orange; Dr in blue; whiskers indicate standard deviation. **C**) Combination of all overall intensity-values (bars in diagrams above) to show significant differences between species and between organs along lifespan. Scale bar: 500 µm.

the number of positive cells as well as their staining intensity is very low. Both parameters rise significantly during childhood and adolescence, followed by a decrease at adulthood and an increase towards later life (Figures 1 and 2 B,C; Supplementary Figures 1A and 2A). While the intensities in zebrafish are much lower than in killifish, the increase in intensity of the positive cells reaches a similar level with age.

SA-ßGal staining in the kidney

The anatomy of the kidney is different in the two species. The kidneys of the zebrafish are structured in a head and a trunk region, while the kidney of the killifish represents the type of head kidney without caudal extension. In both species, the kidneys contain nephrons consisting of glomeruli and proximal and distal tubules merging into collective ducts. In addition, the kidneys of both species exhibit prominent hematopoietic activity and contain endocrine tissue corresponding to the mammalian adrenal gland. The structure of zebrafish kidneys is well characterized at the molecular level. Detailed ultrastructural morphology is lacking in zebrafish and killifish. We have observed substantial SA-ßGal staining of the killifish kidneys (Figure 4C). The staining occurs predominantly in some but not all tubules, but not in the glomeruli, and it is absent in endocrine tissue and occurs only sporadically in hematopoietic cells. This differs from mammals, where several cell types of the kidney were reported to become senescent with age and disease.[70,71] We found it difficult to clearly identify which tubule segment was stained based on morphological criteria. Therefore, we injected fluorescently labelled dextran into killifish, which is known to be preferentially enriched in proximal tubules in many species, including zebrafish.[58] The combination of dextran labelling with SA-ßGal staining demonstrated that SA-ßGal-positive tubules represent a subsection of proximal tubules (Figure 4F). Since not all dextran-labelled tubules were also SA-ßGal stained (but all SA-ßGal stained tubules were dextran-positive), further analysis is required to study whether SA-ßGal staining can be allocated to specific segments of proximal tubules or whether it represents a dynamic progress of senescence during life. Fine structural observation revealed that SA-ßGal staining occurred predominantly in the apical part of tubular epithelial cells and signs of secretion into the tubular lumen were observed (Figure 4 D,E). Overall signal intensities were low in newborns and increased significantly during adolescence, followed by the typical attenuation at adult-

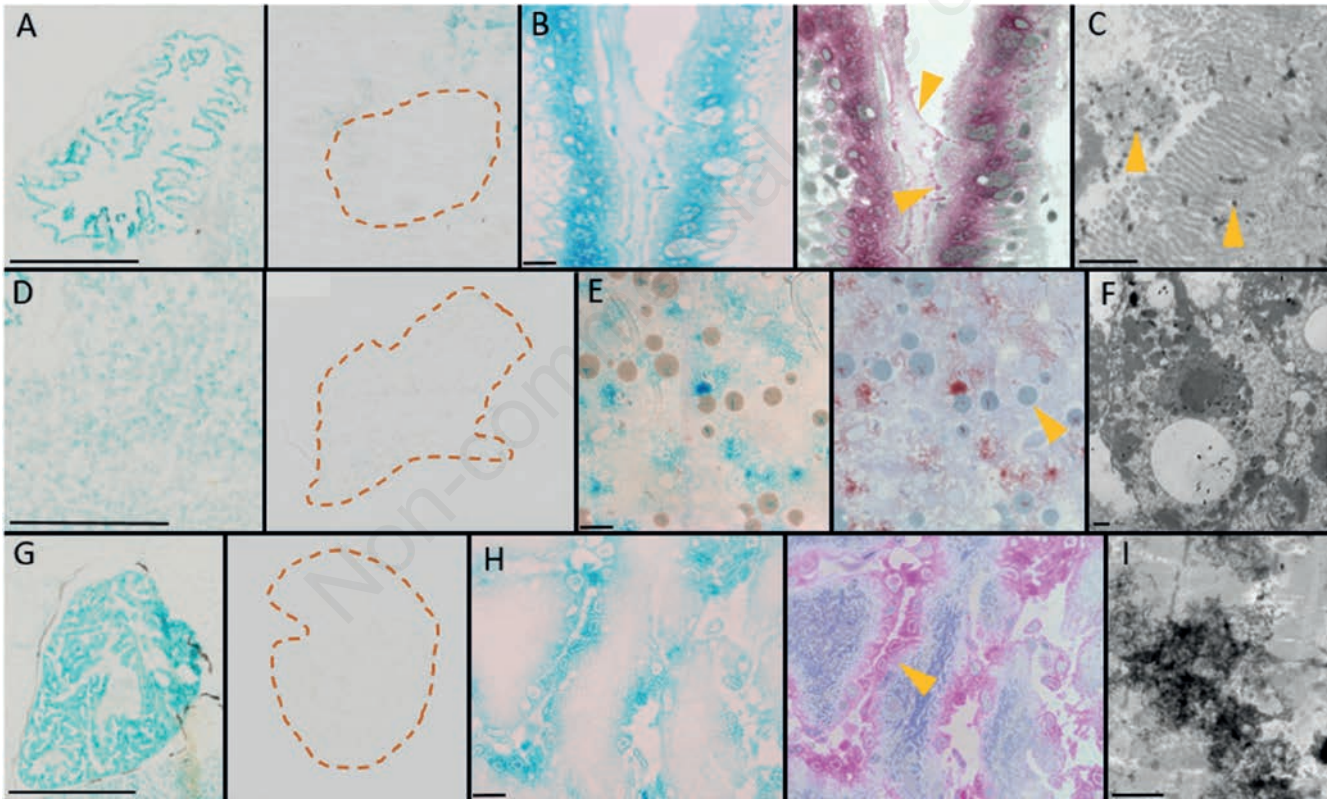

Figure 3. SA-ßGal staining in killifish (Nf) and zebrafish (Dr) organs; representative images. **A**) left Nf child intestine (3 weeks), cryosections, right Dr child intestine (6 weeks); dashed line: organ outline (based on DAPI image; *not shown*). **B**) adult Nf intestine (12 weeks), semithin section; left SA-ßGal staining only; right overlay of SA-ßGal (red; false color) with toluidine blue; note intense staining in apical portions of enterocytes and goblet cells; some staining is also present in the remnant mucus lining of the epithelium (arrowheads). **C**) SA-ßGal staining of adult Nf intestine (12 weeks) at the EM level; precipitates can be seen in the cytoplasm, in the brush border and also in the intestinal lumen (arrowhead). **D**) left Nf child liver (3 weeks), cryosections, right Dr adolescent liver (6 months). **E**) adult Nf liver, semithin section; left SA-ßGal staining only; right overlay of SA-ßGal (red; false color) with toluidine blue; strong staining in hepatocytes (lipid droplets typical for Nf livers are also present (arrowhead)). **F**) SA-ßGal staining in adult Nf liver (12 weeks) at the EM level; precipitates can be seen in a hepatocyte. **G**) left Nf child heart (3 weeks), cryosections, right Dr adolescent heart (6 months). **H**) adult Nf heart, semithin section; left SA-ßGal staining only; right overlay of SA-ßGal (red; false color) with toluidine blue; note very prominent staining of endocardial endothelial cells, whereas staining is only present at the periphery of myocytes (arrowhead). **I**) SA-ßGal staining in adult Nf heart myocardium (12 weeks) at the EM level; precipitates can be seen among sarcomeres. Scale bars: A,D,G) 500 µm; B,E,H) 10 µm; C,F,I) 1 µm.

hood and a sharp increase in old age. Again, the overall signal intensity was much lower in zebrafish than in killifish (Figures 1 and 2 B,C; Supplementary Figures 1A and 2A). However, the signal intensity of positive cells increases much more with age in zebrafish reaching similar values as in killifish at old age.

SA-ßGal staining in the skeletal muscle

Old killifish have reduced locomotion abilities, which is why killifish is also a model system for sarcopenia research. Therefore, we expected significant differences during the aging process in skeletal muscle tissue. Until adulthood, we found no detectable

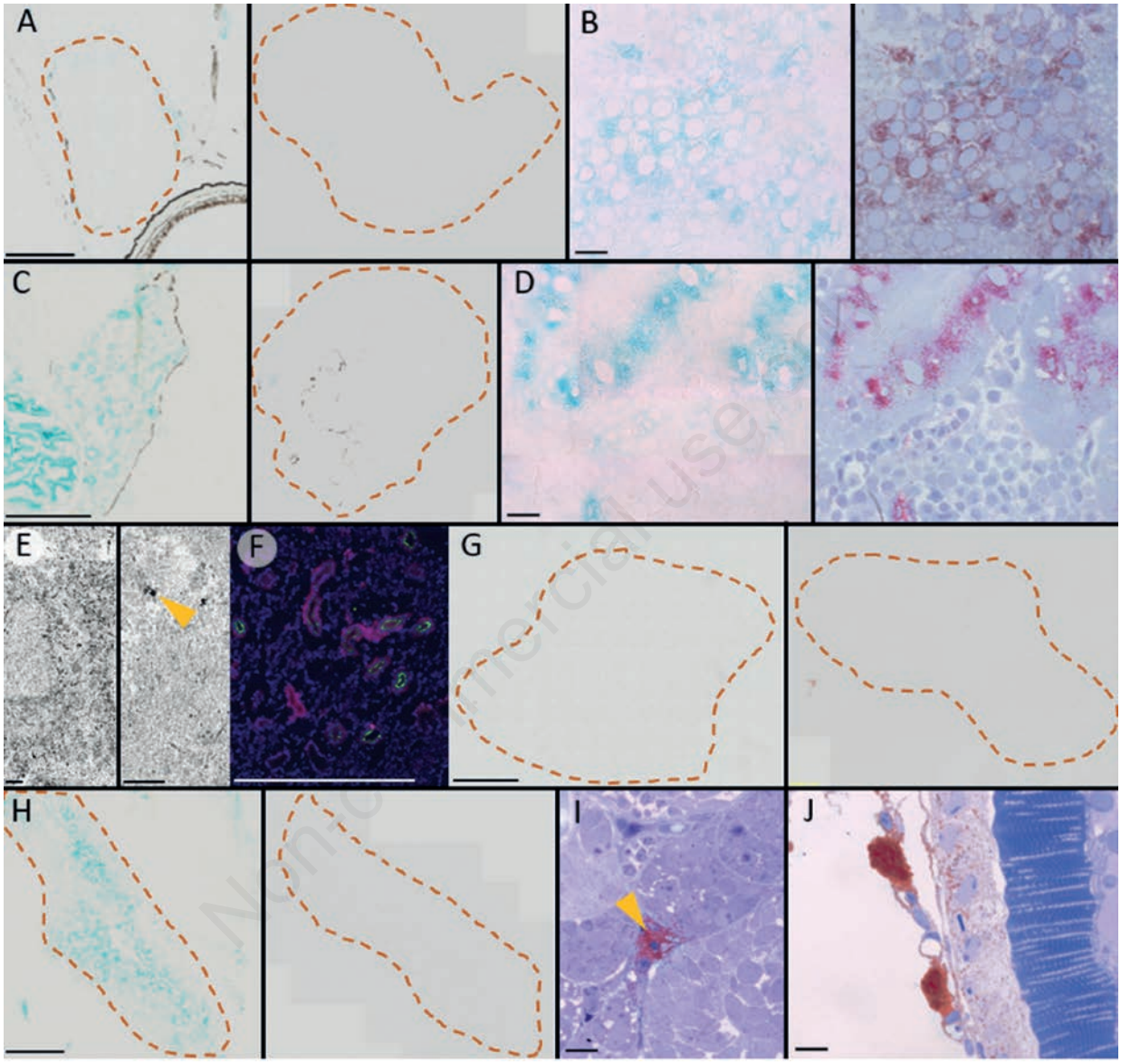

Figure 4. SA-ßGal staining in killifish (Nf) and zebrafish (Dr) organs; representative images. **A**) left Nf adolescent brain (5 weeks), cryosections, right Dr adolescent brain (6 months); dashed line: organ outline (based on DAPI image; not shown). **B**) adult Nf brain (12 weeks), semithin section; left SA-ßGal staining only; right overlay of SA-ßGal (red; false color) with toluidine blue; note staining in some neurons. **C**) left Nf adolescent kidney (5 weeks), cryosection, right Dr adolescent kidney (6 months); dashed line: organ outline (based on DAPI image; not shown). **D**) adult Nf kidney (12 weeks), semithin section; left SA-ßGal staining only; right overlay of SA-ßGal (red; false color) with toluidine blue; note staining in tubular cells, while only little staining is present in the surrounding hematopoietic area. **E**) SA-ßGal staining of adult Nf kidney (12 weeks) at the EM level; left center part of tubular cell; right apical portion of same cell showing brush border typical of proximal tubules; precipitates can be seen in the cytoplasm, in the brush border and also in the tubular lumen (arrowhead). **F**) Adult Nf kidney (12 weeks) after injection with dextran (red) to indicate proximal tubules; overlay with SA-ßGal staining (green; false color) demonstrates that staining is present in proximal tubules. **G**) left skeletal muscle of old Nf (18 weeks), cryosections, right skeletal muscle of old Dr (26 months); dashed line: organ outline (based on DAPI image; not shown). **H**) left Nf adult gonad (testis; 12 weeks), cryosections, right Dr adult gonad (testis; 15 months); dashed line: organ outline (based on DAPI image; not shown). **I**) adult Nf testis (12 weeks), semithin section; overlay of SA-ßGal (red; false color) with toluidine blue; note presence of staining in the testicular stroma (arrowhead). **J**) adult Nf ovary (12 weeks), semithin section; overlay of SA-ßGal (red; false color) with toluidine blue; note presence of staining in the ovarian stroma next to a follicle (granulosa and chorion). Scale bars: A,C,G,H) 500 µm; B,D,I,J) 10 µm; E) 1 µm.

staining in skeletal muscles of killifish. At old age, a substantial increase in positivity was observed, albeit at intensity levels lower than in other organs. Future studies will make it possible to faithfully attribute these positive cells to either myonuclei or satellite cells. The intensity in skeletal muscle of the zebrafish is consistently very low throughout lifetime (Figures 1, 2 B,C and 4G; Supplementary Figures 1A and 2A).

SA-ßGal staining in the gonads

The anatomy of the killifish gonads is similar to that of zebrafish. Fertility rates are subjected to age-related changes in both species, reaching a maximum in adulthood and declining in old age. In killifish, we evaluated gonads from childhood onwards and in zebrafish from adolescence onwards. At young stages where the sexes could not be reliably distinguished, we used the term gonad and focused on testis in later life. SA-ßGal staining is localized to individual cells of the interstitial connective tissue (Figure 4H,I). These cells are often located in the vicinity of capillaries and probably represent Leydig cells. SA-ßGal staining in killifish recapitulates the general pattern with an increase of overall intensity during adolescence, a decrease in adulthood and a significant increase at old age. Signal intensities in killifish are however lower in gonads when compared with other organs. In zebrafish, the staining increases until adulthood and then decreases towards old age. Although this signal patterns appears to be different from that of killifish, it should be noted that the staining in zebrafish gonads is generally very low (Figures 1, 2 B,C; Supplementary Figures 1A and 2A). In killifish, we also performed SA-ßGal reaction in adult ovaries. Accumulations of stained cells were found in the interfollicular stroma of ovaries, often in the vicinity of blood vessels, but not in follicles (Figure 4J). The nature of the stained cells is currently unclear, but morphologically they appear to belong to different cell populations, which could include endocrine stromal cells, monocytes, macrophages or mast cells.[72] The pattern of ovarian staining resembles that found in ovaries of *N. guentheri*, where an increase over age has been observed.[54]

Sex-dependent SA-ßGal staining

Differences in organs of both sexes were analyzed at adult stage of the killifish. At this stage, we found no significant differences between the two sexes in the intensities of the whole organ and of the positive cells. The only distinct exception detected was the proportion of positive cells of all cells in liver, which is significantly higher in males than in females (Supplementary Figure 1B). A subtle difference in the distribution of staining was observed in the kidney. Female killifish kidneys showed a broader spectrum of positively labelled tubules and more frequently and intensely labelled hematopoietic cells than male kidneys (*data not shown*). This however had no effect on the measured intensities (*i.e.*, the intensities of the whole organ and the positive cells). Comparison of ovary and testis showed presence of stained cells in stromal tissue in both cases but no signal in follicles and testicular tubules (Figure 4 I,J). The lack of sex-specific SA-ßGal staining is reminiscent of a recent RNASeq study in killifish brain, heart and skeletal muscle, which showed that age has a greater impact on gene expression than sex.[73]

SA-ßGal staining in other tissues

Other stained tissues that were occasionally observed in killifish, but not quantified and not followed through life, included the spinal cord with a generally stronger signal than in the brain, the skin with increasing numbers and intensities of positive cells, the gills, the epithelial lining of the pharyngeal cavity, the ureter, the lens, the mesothelium, the meninges and the thyroid gland (*data not shown*). Tissues that were not or only weakly stained in killifish included connective tissue, smooth muscle, bone and cartilage, pancreas (exocrine), pseudobranch, air and gall bladder, and retina (*data not shown*). Zebrafish displayed conspicuous signal in the lens, which was the only tissue observed that showed staining in zebrafish at an earlier stage (newborn stage) than in killifish (Supplementary Figure 2A, section intestine, newborn).

Discussion

We found a tissue-specific SA-ßGal staining pattern across organs in terms of the proportion of positive cells and the intensity of stained organs and cells. Tissue-specific variations of senescence have been reported in several mammalian species.[12,15,74-76] We also found that the organ-specific patterns were almost identical in both species studied, but the onset of staining varied dramatically between the two species at the selected ages. While the measured parameters of zebrafish and killifish tended to converge at old age, the signal at younger ages differed markedly. Those organs of zebrafish that show staining show a more gradual increase during the aging process, which is consistent with an earlier report on SA-ßGal staining of whole animals.[42] In killifish, however, organs that are positive in newborns show different signal during lifetime. Some organs show a gradual increase starting from a higher level than in zebrafish (*e.g.*, kidney, brain), while others maintain strong staining from newborns throughout life (*e.g.*, heart). The reasons for this marked difference in SA-ßGal staining between the short and the long-lived species remain speculative. A recent genomic study in killifish concluded that a relaxation of purifying selection is responsible for the accumulation of deleterious mutations in key life-history determining genes caused by genetic bottlenecks during the evolution of this annual species.[77] In this context, our findings of early and strong SA-ßGal staining in killifish are consistent with this study, confirming the genoprotective nature of senescence. The latter is most notable in the heart, where the interspecies difference is striking. The reasons for this remarkably different staining remain speculative for the moment. Indeed, senescence has been described in cardiomyocytes of mice, and has been related to cardiovascular diseases.[78] In addition to cardiomyocytes, senescence has also been detected in heart fibroblasts and vascular endothelial cells,[79,80] but to our knowledge, endocardial senescence has not been reported so far. In terms of tissue distribution, we find signal predominantly in epithelial cells rather than in other tissue types. For example, connective tissue was almost never stained to a detectable extent, which differs from *in vitro* fibroblast cultures in zebrafish[66] and from what has been reported in mammals, *e.g.*, in the case of the heart (see above). In contrast, many of the cells positive for SA-ßGal are terminally differentiated cells such as enterocytes and goblet cells of the epithelial lining of intestinal folds. The cause for SA-ßGal positivity in these differentiated cells is unclear. Recent unpublished data from our lab suggest that cell replenishment in the intestinal epithelium of killifish is reduced with age, leading us to speculate that senescence may have a beneficial function in maintaining tissue integrity, perhaps triggered by stem cell exhaustion. Further studies on senescence in the intestinal epithelium will also be rewarding as it will allow one to study the plasticity of the senescence and apoptosis programs, as apoptosis is the inevitable endpoint of the previously senescent cells. At subcellular level, SA-ßGal staining in polarized cells was predominately present at the apical and in some tissues at the basal parts of the cells, consistent with the secretory nature of SASP and it would also be in line with the reported bystander effect that triggers senescence in neighboring cells *via* paracrine secretion, shown in mice and zebrafish[30,31] and in the mammalian heart.[78] In the case of the heart, we could see staining consistent with such a

bystander effect, as SA-ßGal appears to leak into neighboring cardiomyocytes. Here, the signal was associated with muscle fibrils, suggesting an effect on contractility. However, we also saw staining on the apical surface and in the cardiac lumen, suggesting secretion into the bloodstream. Similar secretion into the lumen were observed in the intestine, renal tubules and in the liver into the circulation. The situation in the heart and liver raises the interesting question of whether the SASP "bystander" effect is limited to local, paracrine secretion to neighboring cells or if it can have a systemic effect on the entire organism.

In conclusion, our observation of intense SA-ßGal staining from a very early age onwards in the short-lived killifish sheds light on the progression and possible heterogeneous functions of cellular senescence in an organism that develops very rapidly to reach sexual maturity, which has been shaped by evolutionary selection pressure in the species natural habitat of temporary pools. The fast growth of killifish to reach sexual maturity appears to be at the cost of cellular repair mechanisms,[77] and in this context it can be speculated that the observed early onset of cellular senescence may help to mitigate deleterious effects of cellular damage. In contrast, SA-ßGal staining of terminally differentiated cells may reflect an important function in maintaining structural tissue homeostasis, pointing to different roles that cellular senescence may play in killifish. Overall, we hope that the presented organ-specific map of SA-ßGal staining in killifish will be useful for further studies with this exciting model system for aging research.

References

1. Lopez-Otin C, Blasco MA, Partridge L, Serrano M, Kroemer G. Hallmarks of aging: An expanding universe. Cell 2023; 186:243-78.
2. Hayflick L, Moorhead PS. The serial cultivation of human diploid cell strains. Exp Cell Res 1961;25:585-621.
3. Hernandez-Segura A, Nehme J, Demaria M. Hallmarks of cellular senescence. Trends Cell Biol 2018;28:436-53.
4. Campisi J. Aging, cellular senescence, and cancer. Annu Rev Physiol 2013;75:685-705.
5. Childs BG, Durik M, Baker DJ, van Deursen JM. Cellular senescence in aging and age-related disease: From mechanisms to therapy. Nat Med 2015;21:1424-35.
6. He S, Sharpless NE. Senescence in health and disease. Cell 2017;169:1000-11.
7. Herranz N, Gil J. Mechanisms and functions of cellular senescence. J Clin Invest 2018;128:1238-46.
8. Kowald A, Passos JF, Kirkwood TBL. On the evolution of cellular senescence. Aging Cell 2020;19:e13270.
9. Roger L, Tomas F, Gire V. Mechanisms and regulation of cellular senescence. Int J Mol Sci 2021;22:13173.
10. Schwartz RE, Conboy IM. Non-intrinsic, systemic mechanisms of cellular senescence. Cells 2023;12:2769.
11. Singh PP, Demmitt BA, Nath RD, Brunet A. The genetics of aging: A vertebrate perspective. Cell 2019;177:200-20.
12. Baker DJ, Childs BG, Durik M, Wijers ME, Sieben CJ, Zhong J, et al. Naturally occurring p16(ink4a)-positive cells shorten healthy lifespan. Nature 2016;530:184-9.
13. Biran A, Zada L, Abou Karam P, Vadai E, Roitman L, Ovadya Y, et al. Quantitative identification of senescent cells in aging and disease. Aging Cell 2017;16:661-71.
14. Burd CE, Sorrentino JA, Clark KS, Darr DB, Krishnamurthy J, Deal AM, et al. Monitoring tumorigenesis and senescence in vivo with a p16(ink4a)-luciferase model. Cell 2013;152:340-51.
15. Xu P, Wang M, Song WM, Wang Q, Yuan GC, Sudmant PH, et al. The landscape of human tissue and cell type specific expression and co-regulation of senescence genes. Mol Neurodegener 2022;17:5.
16. Avelar RA, Ortega JG, Tacutu R, Tyler EJ, Bennett D, Binetti P, et al. A multidimensional systems biology analysis of cellular senescence in aging and disease. Genome Biol 2020;21:91.
17. Xu M, Pirtskhalava T, Farr JN, Weigand BM, Palmer AK, Weivoda MM, et al. Senolytics improve physical function and increase lifespan in old age. Nat Med 2018;24:1246-56.
18. de Keizer PL. The fountain of youth by targeting senescent cells? Trends Mol Med 2017;23:6-17.
19. Ovadya Y, Krizhanovsky V. Strategies targeting cellular senescence. J Clin Invest 2018;128:1247-54.
20. Chaib S, Tchkonia T, Kirkland JL. Cellular senescence and senolytics: The path to the clinic. Nat Med 2022;28:1556-68.
21. Zhang L, Pitcher LE, Prahalad V, Niedernhofer LJ, Robbins PD. Targeting cellular senescence with senotherapeutics: Senolytics and senomorphics. FEBS J 2023;290:1362-83.
22. Demaria M, Ohtani N, Youssef SA, Rodier F, Toussaint W, Mitchell JR, et al. An essential role for senescent cells in optimal wound healing through secretion of pdgf-aa. Dev Cell 2014;31:722-33.
23. Gal H, Lysenko M, Stroganov S, Vadai E, Youssef SA, Tzadikevitch-Geffen K, et al. Molecular pathways of senescence regulate placental structure and function. EMBO J 2019;38:e100849.
24. Gibaja A, Aburto MR, Pulido S, Collado M, Hurle JM, Varela-Nieto I, et al. Tgfbeta2-induced senescence during early inner ear development. Sci Rep 2019;9:5912.
25. Ritschka B, Storer M, Mas A, Heinzmann F, Ortells MC, Morton JP, et al. The senescence-associated secretory phenotype induces cellular plasticity and tissue regeneration. Genes Dev 2017;31:172-83.
26. Da Silva-Alvarez S, Guerra-Varela J, Sobrido-Camean D, Quelle A, Barreiro-Iglesias A, Sanchez L, et al. Developmentally-programmed cellular senescence is conserved and widespread in zebrafish. Aging (Albany NY) 2020;12:17895-901.
27. Grosse L, Wagner N, Emelyanov A, Molina C, Lacas-Gervais S, Wagner KD, et al. Defined p16(high) senescent cell types are indispensable for mouse healthspan. Cell Metab 2020;32:87-99.e6.
28. Blagosklonny MV. Cell senescence, rapamycin and hyperfunction theory of aging. Cell Cycle 2022;21:1456-67.
29. Coppe JP, Desprez PY, Krtolica A, Campisi J. The senescence-associated secretory phenotype: The dark side of tumor suppression. Annu Rev Pathol 2010;5:99-118.
30. da Silva PFL, Ogrodnik M, Kucheryavenko O, Glibert J, Miwa S, Cameron K, et al. The bystander effect contributes to the accumulation of senescent cells in vivo. Aging Cell 2019;18:e12848.
31. Nelson G, Wordsworth J, Wang C, Jurk D, Lawless C, Martin-Ruiz C, et al. A senescent cell bystander effect: Senescence-induced senescence. Aging Cell 2012;11:345-9.
32. Cristofalo VJ. SA beta gal staining: Biomarker or delusion. Exp Gerontol 2005;40:836-8.
33. Sikora E, Bielak-Zmijewska A, Mosieniak G. A common signature of cellular senescence; does it exist? Ageing Res Rev 2021;71:101458.
34. Dimri GP, Lee X, Basile G, Acosta M, Scott G, Roskelley C, et al. A biomarker that identifies senescent human cells in culture and in aging skin in vivo. Proc Natl Acad Sci USA 1995;92:9363-7.
35. Itahana K, Campisi J, Dimri GP. Methods to detect biomarkers of cellular senescence: The senescence-associated beta-galac-

tosidase assay. Methods Mol Biol 2007;371:21-31.
36. Marzullo M, Mai ME, Ferreira MG. Whole-mount senescence-associated beta-galactosidase (sa-beta-gal) activity detection protocol for adult zebrafish. Bio Protoc 2022;12:e4457.
37. Lee BY, Han JA, Im JS, Morrone A, Johung K, Goodwin EC, et al. Senescence-associated beta-galactosidase is lysosomal beta-galactosidase. Aging Cell 2006;5:187-95.
38. Kurz DJ, Decary S, Hong Y, Erusalimsky JD. Senescence-associated (beta)-galactosidase reflects an increase in lysosomal mass during replicative ageing of human endothelial cells. J Cell Sci 2000;113:3613-22.
39. Van Houcke J, De Groef L, Dekeyster E, Moons L. The zebrafish as a gerontology model in nervous system aging, disease, and repair. Ageing Res Rev 2015;24:358-68.
40. Gerhard GS. Comparative aspects of zebrafish (Danio rerio) as a model for aging research. Exp Gerontol 2003;38:1333-41.
41. Valenzano DR, Terzibasi E, Cattaneo A, Domenici L, Cellerino A. Temperature affects longevity and age-related locomotor and cognitive decay in the short-lived fish nothobranchius furzeri. Aging cell 2006;5:275-8.
42. Kishi S, Uchiyama J, Baughman AM, Goto T, Lin MC, Tsai SB. The zebrafish as a vertebrate model of functional aging and very gradual senescence. Exp Gerontol 2003;38:777-86.
43. Tsai SB, Tucci V, Uchiyama J, Fabian NJ, Lin MC, Bayliss PE, et al. Differential effects of genotoxic stress on both concurrent body growth and gradual senescence in the adult zebrafish. Aging Cell 2007;6:209-24.
44. Novoa B, Pereiro P, Lopez-Munoz A, Varela M, Forn-Cuni G, Anchelin M, et al. Rag1 immunodeficiency-induced early aging and senescence in zebrafish are dependent on chronic inflammation and oxidative stress. Aging Cell 2019;18:e13020.
45. El Mai M, Marzullo M, de Castro IP, Ferreira MG. Opposing p53 and mtor/akt promote an in vivo switch from apoptosis to senescence upon telomere shortening in zebrafish. Elife 2020;9:e54935.
46. Arslan-Ergul A, Erbaba B, Karoglu ET, Halim DO, Adams MM. Short-term dietary restriction in old zebrafish changes cell senescence mechanisms. Neuroscience 2016;334:64-75.
47. Henriques CM, Carneiro MC, Tenente IM, Jacinto A, Ferreira MG. Telomerase is required for zebrafish lifespan. PLoS Genet 2013;9:e1003214.
48. Van Houcke J, Marien V, Zandecki C, Vanhunsel S, Moons L, Ayana R, et al. Aging impairs the essential contributions of non-glial progenitors to neurorepair in the dorsal telencephalon of the killifish nothobranchius furzeri. Aging Cell 2021;20:e13464.
49. de Bakker DEM, Valenzano DR. Turquoise killifish: A natural model of age-dependent brain degeneration. Ageing Res Rev 2023;90:102019.
50. Genade T, Benedetti M, Terzibasi E, Roncaglia P, Valenzano DR, Cattaneo A, et al. Annual fishes of the genus nothobranchius as a model system for aging research. Aging Cell 2005;4:223-33.
51. Graf M, Hartmann N, Reichwald K, Englert C. Absence of replicative senescence in cultured cells from the short-lived killifish nothobranchius furzeri. Exp Gerontol 2013;48:17-28.
52. Song L, Li C, Wu F, Zhang S. Dietary intake of diosgenin delays aging of male fish nothobranchius guentheri through modulation of multiple pathways that play prominent roles in ros production. Biogerontology 2022;23:201-13.
53. Li S, Hou Y, Liu K, Zhu H, Qiao M, Sun X, et al. Metformin protects against inflammation, oxidative stress to delay poly i:C-induced aging-like phenomena in the gut of an annual fish. J Gerontol A Biol Sci Med Sci 2022;77:276-82.
54. Zhu H, Li X, Qiao M, Sun X, Li G. Resveratrol alleviates inflammation and er stress through sirt1/nrf2 to delay ovarian aging in a short-lived fish. J Gerontol A Biol Sci Med Sci 2023;78:596-602.
55. Kimmel CB, Ballard WW, Kimmel SR, Ullmann B, Schilling TF. Stages of embryonic development of the zebrafish. Dev Dyn 1995;203:253-310.
56. Zupkovitz G, Kabiljo J, Kothmayer M, Schlick K, Schofer C, Lagger S, et al. Analysis of methylation dynamics reveals a tissue-specific, age-dependent decline in 5-methylcytosine within the genome of the vertebrate aging model nothobranchius furzeri. Front Mol Biosci 2021;8:627143.
57. Gilbert MJ, Zerulla TC, Tierney KB. Zebrafish (Danio rerio) as a model for the study of aging and exercise: Physical ability and trainability decrease with age. Exp Gerontol 2014;50:106-13.
58. McCampbell KK, Springer KN, Wingert RA. Analysis of nephron composition and function in the adult zebrafish kidney. J Vis Exp 2014:e51644.
59. Gonzalez-Gualda E, Baker AG, Fruk L, Munoz-Espin D. A guide to assessing cellular senescence in vitro and in vivo. FEBS J 2021;288:56-80.
60. Gioglio L, Cusella de AM, Boratto R, Poggi P. An improved method for beta-galactosidase activity detection on muscle tissue. A light and electron microscopic study. Ann Anat 2002;184:153-7.
61. Menke AL, Spitsbergen JM, Wolterbeek AP, Woutersen RA. Normal anatomy and histology of the adult zebrafish. Toxicol Pathol 2011;39:759-75.
62. Dyková I, Zák J, Blazek R, Reichard M, Soucková K, Slaby O. Histology of major organ systems of Nothobranchius fishes: Short-lived model species. J Vertebr Biol 2022;71:21074.
63. Allred DC, Harvey JM, Berardo M, Clark GM. Prognostic and predictive factors in breast cancer by immunohistochemical analysis. Mod Pathol 1998;11:155-68.
64. Schindelin J, Arganda-Carreras I, Frise E, Kaynig V, Longair M, Pietzsch T, et al. Fiji: An open-source platform for biological-image analysis. Nature methods 2012;9:676-82.
65. Borgonovo J, Allende-Castro C, Medinas DB, Cardenas D, Cuevas MP, Hetz C, et al. Immunohistochemical characterisation of the adult nothobranchius furzeri intestine. Cell Tissue Res 2024;395:21-38.
66. Fathi E, Farahzadi R, Sheikhzadeh N. Immunophenotypic characterization, multi-lineage differentiation and aging of zebrafish heart and liver tissue-derived mesenchymal stem cells as a novel approach in stem cell-based therapy. Tissue Cell 2019;57:15-21.
67. Bowley G, Kugler E, Wilkinson R, Lawrie A, van Eeden F, Chico TJA, et al. Zebrafish as a tractable model of human cardiovascular disease. Br J Pharmacol 2022;179:900-17.
68. Jensen B, Agger P, de Boer BA, Oostra RJ, Pedersen M, van der Wal AC, et al. The hypertrabeculated (noncompacted) left ventricle is different from the ventricle of embryos and ectothermic vertebrates. Biochim Biophys Acta 2016;1863:1696-706.
69. Kenney JW, Steadman PE, Young O, Shi MT, Polanco M, Dubaishi S, et al. A 3D adult zebrafish brain atlas (AZBA) for the digital age. Elife 2021;10:e69988.
70. Huang W, Hickson LJ, Eirin A, Kirkland JL, Lerman LO. Cellular senescence: The good, the bad and the unknown. Nat Rev Nephrol 2022;18:611-27.
71. Docherty MH, O'Sullivan ED, Bonventre JV, Ferenbach DA. Cellular senescence in the kidney. J Am Soc Nephrol 2019;30:726-36.
72. Mohamedien D, Mokhtar DM, Abdellah N, Awad M, Albano M, Sayed RKA. Ovary of zebrafish during spawning season:

Ultrastructure and immunohistochemical profiles of sox9 and myostatin. Animals (Basel) 2023;13:3362.
73. Xu A, Teefy BB, Lu RJ, Nozownik S, Tyers AM, Valenzano DR, et al. Transcriptomes of aging brain, heart, muscle, and spleen from female and male african turquoise killifish. Sci Data 2023;10:695.
74. Wang C, Jurk D, Maddick M, Nelson G, Martin-Ruiz C, von Zglinicki T. DNA damage response and cellular senescence in tissues of aging mice. Aging Cell 2009;8:311-23.
75. Tuttle CSL, Waaijer MEC, Slee-Valentijn MS, Stijnen T, Westendorp R, Maier AB. Cellular senescence and chronological age in various human tissues: A systematic review and meta-analysis. Aging Cell 2020;19:e13083.
76. Krishnamurthy J, Torrice C, Ramsey MR, Kovalev GI, Al-Regaiey K, Su L, et al. Ink4a/arf expression is a biomarker of aging. J Clin Invest 2004;114:1299-307.
77. Cui R, Medeiros T, Willemsen D, Iasi LNM, Collier GE, Graef M, et al. Relaxed selection limits lifespan by increasing mutation load. Cell 2019;178:385-99 e20.
78. Anderson R, Lagnado A, Maggiorani D, Walaszczyk A, Dookun E, Chapman J, et al. Length-independent telomere damage drives post-mitotic cardiomyocyte senescence. EMBO J 2019;38:e100492.
79. Mehdizadeh M, Aguilar M, Thorin E, Ferbeyre G, Nattel S. The role of cellular senescence in cardiac disease: Basic biology and clinical relevance. Nat Rev Cardiol 2022;19:250-64.
80. Chen MS, Lee RT, Garbern JC. Senescence mechanisms and targets in the heart. Cardiovasc Res 2022;118:1173-87.

Online supplementary material:

Figure 1. Quantitative measurement of staining intensities in killifish and zebrafish.

Figure 2. SA-βGal staining throughout the lifespan of killifish and zebrafish.

Received: 25 January 2024. Accepted: 21 February 2024.

Licensee PAGEPress, Italy
European Journal of Histochemistry 2024; 68:3977
doi:10.4081/ejh.2024.3977